Extreme One-Dimensional Modeling for Computational Hemodynamics

PJ Blanco, LO Müller, MS Watanabe & RA Feijóo

Petrópolis, Brazil

Fourth Workshop of the CNPq-Inria HOSCAR Project:
HPC and Scientific Data Management Driven by Highly Demanding Applications

UFRGS – Gramado

September, 2014

Table of contents

Scientific challenge in modeling physiological systems

- Understanding interactions
- Onset and progress of diseases
- Diagnosis of pathological conditions
- Surgical planning
- Treatment strategies

In generic or patient-specific settings

Scientific challenge in modeling physiological systems

- Understanding interactions
- Onset and progress of diseases
- Diagnosis of pathological conditions
- Surgical planning
- Treatment strategies

In generic or patient-specific settings

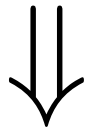

Simulate the interplay among multiscale and multisystem phenomena

One-dimensional blood flow modeling in a nutshell

- Early theoretical developments
  [Lambert'56; Barnard'66; Taylor'66; Hughes'73; Kivity'74]
- Early topological descriptions
  [Spencer'59; Noordergraaf'63; Westerhof'69; Anliker'71; Schaaf'72]
- Subsequent improvements and alternatives
  [Avolio'80; Stettler'81; Stergiopulos'92; Sherwin'03; Wang'04]
- Further validations/verifications (in vitro/in vivo/in silico)
  [Olufsen'00; Matthys'07; Reymond'09; Alastruey'11; Grinberg'11; Reymond'11]

One-dimensional blood flow modeling in a nutshell

- Early theoretical developments

  [Lambert'56; Barnard'66; Taylor'66; Hughes'73; Kivity'74]

- Early topological descriptions

  [Spencer'59; Noordergraaf'63; Westerhof'69; Anliker'71; Schaaf'72]

- Subsequent improvements and alternatives

  [Avolio'80; Stettler'81; Stergiopulos'92; Sherwin'03; Wang'04]

- Further validations/verifications (in vitro/in vivo/in silico)

  [Olufsen'00; Matthys'07; Reymond'09; Alastruey'11; Grinberg'11; Reymond'11]

One-dimensional blood flow modeling in a nutshell

- Early theoretical developments

  [Lambert'56; Barnard'66; Taylor'66; Hughes'73; Kivity'74]

- Early topological descriptions

  [Spencer'59; Noordergraaf'63; Westerhof'69; Anliker'71; Schaaf'72]

- Subsequent improvements and alternatives

  [Avolio'80; Stettler'81; Stergiopulos'92; Sherwin'03; Wang'04]

- Further validations/verifications (in vitro/in vivo/in silico)

  [Olufsen'00; Matthys'07; Reymond'09; Alastruey'11; Grinberg'11; Reymond'11]

One-dimensional blood flow modeling in a nutshell

- Early theoretical developments

  [Lambert'56; Barnard'66; Taylor'66; Hughes'73; Kivity'74]
- Early topological descriptions

  [Spencer'59; Noordergraaf'63; Westerhof'69; Anliker'71; Schaaf'72]
- Subsequent improvements and alternatives

  [Avolio'80; Stettler'81; Stergiopulos'92; Sherwin'03; Wang'04]
- Further validations/verifications (in vitro/in vivo/in silico)

  [Olufsen'00; Matthys'07; Reymond'09; Alastruey'11; Grinberg'11; Reymond'11]

Sorry for missing references!

Mathematical model

Incompressible flow of Newtonian fluid in compliant vessels

$$\begin{cases} \partial_t A + \partial_x q = 0 \\ \partial_t q + \partial_x \left(\hat{\alpha} \dfrac{q^2}{A} \right) + \dfrac{A}{\rho} \partial_x p = f \end{cases}$$

Constitutive relation for the vessel wall

$$p(x,t) = \underbrace{p_0}_{\text{reference}} + \underbrace{\zeta(x,t)}_{\text{tube law}}$$

$$\zeta(x,t) = \frac{\pi R_0 h_0}{A} [\underbrace{E_e \varepsilon}_{\text{elastin}} + \underbrace{E_c \epsilon_r \ln(e^{\chi} + 1)}_{\textit{collagen}} + \underbrace{\frac{K_m}{2\sqrt{A A_0}} \frac{\partial A}{\partial t}}_{\text{smooth muscle}}]$$

$$\varepsilon = \sqrt{\frac{A}{A_o}} - 1 \qquad \chi = \frac{\varepsilon - \varepsilon_o}{\epsilon_r}$$

Mathematical model

At bifurcations (N_T converging segments)

$$\sum_{i=1}^{N_T} q_i = 0$$

$$p_i + \frac{1}{2}\rho u_i^2 = p_1 + \frac{1}{2}\rho u_1^2 \quad 2, \ldots, N_T$$

At terminal segments (Windkessel model)

$$r_A r_B C \frac{dq}{dt} = R_B C \frac{d}{dt}(p - p_T) + (p - p_T) - (R_A + R_B)q$$

Ongoing and future applications

- Regulatory mechanisms: long simulations (hours to days) (Blanco et al., 2012)
- Systemic interactions, drug delivery: long simulations (hours to days)
- Parameter estimation using the unscented Kalman filter: $N + 1$ simultaneous direct problems for the estimation of N parameters (Lombardi, 2013)
- Parameter estimation using variational formulations: forward in time direct problem and backward in time adjoint problem (Martin et al., 2005)
- Uncertainty quantification: stochastic PDEs require a (very) high number of direct problem runs (Chen et al.)

Challenges

- HPC (parallel run or massive number of parallel runs)
- Numerical schemes must be: accurate, efficient and robust and suitable for HPC
- Data management
- Data mining

Overview

Mathematical model reformulation

One-dimensional blood flow equations:

$$\begin{cases} \partial_t A + \partial_x q = 0 \\ \partial_t q + \partial_x \left(\hat{\alpha} \dfrac{q^2}{A} \right) + \dfrac{A}{\rho} \partial_x p = f \end{cases}$$

with

$$p(x,t) = \underbrace{p_0}_{\text{reference}} + \underbrace{\zeta(x,t)}_{\text{tube law}}$$

$$\zeta(x,t) = \frac{\pi R_0 h_0}{A} [\underbrace{E_e \varepsilon}_{\text{elastin}} + \underbrace{E_c \epsilon_r \ln(e^{\chi} + 1)}_{\textit{collagen}} + \underbrace{\frac{K_m}{2\sqrt{A A_0}} \frac{\partial A}{\partial t}}_{\text{smooth muscle}}]$$

$$\varepsilon = \sqrt{\frac{A}{A_o}} - 1 \qquad \chi = \frac{\varepsilon - \varepsilon_o}{\epsilon_r}$$

Mathematical model reformulation

Hyperbolic reformulation

Rewrite the *tube law* as

$$\zeta = \frac{\sqrt{\pi}\sqrt{A_0}h_0}{A}\left[E_e\varepsilon + E_c\epsilon_r \ln\left(e^{\chi}+1\right) - \frac{K_m}{2\sqrt{AA_0}}\theta\right] .$$

introducing the additional equation

$$\partial_t\theta = \frac{1}{T}\left(\partial_x q - \theta\right) ,$$

with T *relaxation time*.

NB

Full details, as well as a criteria for choosing T are found in Montecinos et al. (2014); Montecinos and Toro (2014).

Mathematical model reformulation

Variable mechanical and geometrical properties

The spatial derivative of ζ is

$$\frac{\partial \zeta}{\partial x} = \frac{\partial \zeta}{\partial A}\frac{\partial A}{\partial x} + \underbrace{\frac{\partial \zeta}{\partial A_0}\frac{\partial A_0}{\partial x} + \frac{\partial \zeta}{\partial h_0}\frac{\partial h_0}{\partial x} + \frac{\partial \zeta}{\partial E_e}\frac{\partial E_e}{\partial x} + \frac{\partial \zeta}{\partial E_c}\frac{\partial E_c}{\partial x}}_{\text{geometric source terms}} + \frac{\partial \zeta}{\partial \theta}\frac{\partial \theta}{\partial x}\,.$$

Mathematical model reformulation

We consider the following system

$$\partial_t \mathbf{Q} + \mathbf{A}(\mathbf{Q})\partial_x \mathbf{Q} = \mathbf{S}(\mathbf{Q}),$$

with:

- state vector $\mathbf{Q} = \left[A, q, \theta, A_0, h_0, E_e, E_c, p_e\right]^T$
- coefficient matrix $\mathbf{A}(\mathbf{Q})$
- source vector $\mathbf{S}(\mathbf{Q})$
- additional equations of the type $\partial_t b = 0$, with $b = \{A_0, h_0, E_e, E_c, p_e\}$

For details see Toro and Siviglia (2013).

Path-conservative finite volume schemes

Split the spatial domain in $I_i = [x_{i-\frac{1}{2}}, x_{i+\frac{1}{2}}]$, with $i = 1, \ldots, N$ and integrate in space and time over $[x_{i-\frac{1}{2}}, x_{i+\frac{1}{2}}] \times [t^n, t^{n+1}]$, to obtain

$$\mathbf{Q}_i^{n+1} = \mathbf{Q}_i^n - \frac{1}{\Delta x_i} \int_{t^n}^{t^{n+1}} \int_{x_{i-\frac{1}{2}}}^{x_{i+\frac{1}{2}}} \mathbf{A}(\mathbf{Q}) \partial_x \mathbf{Q} dx dt$$
$$- \frac{\Delta t}{\Delta x_i} \left(\mathbf{D}_{i+\frac{1}{2}}^- + \mathbf{D}_{i-\frac{1}{2}}^+ \right) + \Delta t \mathbf{S}_i \,,$$

where

$$\mathbf{Q}_i^n = \frac{1}{\Delta x_i} \int_{x_{i-\frac{1}{2}}}^{x_{i+\frac{1}{2}}} \mathbf{Q}(x, t^n)\, dx \,,$$

$$\mathbf{S}_i = \frac{1}{\Delta t \Delta x_i} \int_{t^n}^{t^{n+1}} \int_{x_{i-\frac{1}{2}}}^{x_{i+\frac{1}{2}}} \mathbf{S}(\mathbf{Q}(x,t)) dx dt$$

and ...

Fluctuations

Fluctuations

$$\mathbf{D}^{\pm}_{i+\frac{1}{2}} = \frac{1}{\Delta t}\int_{t^n}^{t^{n+1}} \mathcal{D}^{\pm}_{i+\frac{1}{2}}\left(\mathbf{Q}^{-}_{i+\frac{1}{2}}(t), \mathbf{Q}^{+}_{i+\frac{1}{2}}(t), \boldsymbol{\Psi}\right) dt\,,$$

with

$$\mathcal{D}^{\pm}_{i+\frac{1}{2}} = \frac{1}{2}\int_0^1 \left[\mathbf{A}(\boldsymbol{\Psi}(\mathbf{Q}^{-}_{i+\frac{1}{2}}, \mathbf{Q}^{+}_{i+\frac{1}{2}}, s)) \pm |\mathbf{A}(\boldsymbol{\Psi}(\mathbf{Q}^{-}_{i+\frac{1}{2}}, \mathbf{Q}^{+}_{i+\frac{1}{2}}, s))|\right] \frac{\partial \boldsymbol{\Psi}}{\partial s} ds\,,$$

where

- $\boldsymbol{\Psi} = \boldsymbol{\Psi}(\mathbf{Q}^{-}, \mathbf{Q}^{+}, s)$, with $0 \leq s \leq 1$, is a Lipschitz continuous function that connects the left state $\mathbf{Q}^{-}$ to the right state $\mathbf{Q}^{+}$ in phase-space.
- Integral in phase-space performed numerically: Dumbser-Osher-Toro Riemann solver (Dumbser and Toro, 2011)
- $\mathbf{Q}^{\pm}_{i+\frac{1}{2}}(t)$ is the solution of the Generalized Riemann Problem (GRP) at $x_{i+\frac{1}{2}}$

Fluctuations

Non-conservative system:

- the weak solution will depend on the choice of the integration path $\boldsymbol{\Psi}$ (Dal Maso et al., 1995)
- In the original Dumbser-Osher-Toro solver a segment path was proposed

$$\boldsymbol{\Psi}(s) = \mathbf{Q}^{-}_{i+\frac{1}{2}} + s\left(\mathbf{Q}^{+}_{i+\frac{1}{2}} - \mathbf{Q}^{-}_{i+\frac{1}{2}}\right).$$

- Müller and Toro (2013): consider the eigenstructure of the non-conservative system to construct well-balanced schemes using the DOT solver

Spatial reconstruction

Weighted Essentially Non-Oscillatory reconstruction (Jiang and Shu, 1996)

We reconstruct element-wise polynomials of the type

$$\mathbf{w}_i = \mathbf{w}_i(\xi, t^n) = \sum_{l=1}^{M+1} \psi_l(\xi)\hat{\mathbf{w}}_l(t^n) := \psi_l(\xi)\hat{\mathbf{w}}_l(t^n)\,,$$

where

- $\xi = (x - x_{i-\frac{1}{2}})/\Delta x$
- $M = k - 1$ is the polynomial degree of $\mathbf{w}_i$
- k is the **space-time** order of accuracy of the scheme
- $\psi_l(\xi)$ are the corresponding basis functions
- $\hat{\mathbf{w}}_l$ are the expansion coefficients

Spatial reconstruction

The reconstruction stencil is

$$\mathcal{S}_i^s = \bigcup_{e=i-L}^{i+R} T_e \,,$$

- $L(M, s)$ and $R(M, s)$ are the stencil extent to the left and right of the central element T_i,
- We use three fixed reconstruction stencils
- One central stencil ($s = 1$, $L = R = M/2$)
- A fully left-sided stencil ($s = 2$, $L = M$, $R = 0$)
- A fully-right sided stencil ($s = 3$, $L = 0$, $R = M$)
- The reconstructed polynomial has k coefficients and is of degree $M = k - 1$

Spatial reconstruction

Requiring integral conservation in $\mathcal{S}_i^s$

$$\int_{T_j} \mathbf{w}_i^s(\xi, t^n) d\xi = \hat{\mathbf{w}}_l^s(t^n) \int_{T_j} \psi_l(\xi) d\xi = \mathbf{Q}_j^n \quad \forall T_j \in \mathcal{S}_i^s \,.$$

Finally, $\hat{\mathbf{w}}_l^j(t^n)$ are a non-linear combination of the form

$$\hat{\mathbf{w}}_l(t^n) = \sum_{s=1}^{N_s} \omega_s \hat{\mathbf{w}}_l^s(t^n) \,,$$

with non-linear weights

$$\omega_s = \frac{\tilde{\omega}_s}{\tilde{\omega}_0 + \tilde{\omega}_{-k} + \tilde{\omega}_k}, \quad \tilde{\omega}_s = \frac{\lambda_s}{(\sigma_s + \epsilon)^r}$$

and oscillation indicators σ_s are computed as

$$\sum_{l=1}^{M} \int_0^1 \left(\frac{\partial^l}{\partial \xi^l} \mathbf{w}_i^s(\xi, t^n) \right)^2 d\xi \,.$$

Generalized Riemann Problem

The GRP at cell interface $x = x_{i+\frac{1}{2}}$ (locally at $x = 0$)

$$\left.\begin{aligned} &\partial_t \mathbf{Q} + \mathbf{A}(\mathbf{Q})\partial_x \mathbf{Q} = \mathbf{S}(\mathbf{Q}), \quad x \in \mathcal{R}, \quad t > 0, \\ &\mathbf{Q}(x,0) = \begin{cases} \mathbf{w}_i(x) & \text{if } x < 0, \\ \mathbf{w}_{i+1}(x) & \text{if } x > 0. \end{cases} \end{aligned}\right\},$$

NB

The solution of the GRP will yield a time-dependent solution at the interface, locally along $x/t = 0$, and will be used to evaluate integrals in the FV scheme.

Generalized Riemann Problem

The GRP at cell interface $x = x_{i+\frac{1}{2}}$ (locally at $x = 0$)

$$\left.\begin{aligned} &\partial_t \mathbf{Q} + \mathbf{A}(\mathbf{Q})\partial_x \mathbf{Q} = \mathbf{S}(\mathbf{Q}), \quad x \in \mathcal{R}, \quad t > 0, \\ &\mathbf{Q}(x,0) = \begin{cases} \mathbf{w}_i(x) & \text{if } x < 0, \\ \mathbf{w}_{i+1}(x) & \text{if } x > 0. \end{cases} \end{aligned}\right\},$$

NB

The solution of the GRP will yield a time-dependent solution at the interface, locally along $x/t = 0$, and will be used to evaluate integrals in the FV scheme.

Dumbser-Enaux-Toro Solver

Dumbser et al. (2008b)

We work in a reference space-time element $T_E = [0;1] \times [0;1]$ with $\xi = (x - x_{i-\frac{1}{2}})/\Delta x_i$ and $\tau = (t - t^n)/\Delta t$, where the system reads

$$\partial_\tau \mathbf{Q}_h + \mathbf{A}^* \partial_\xi \mathbf{Q}_h = \mathbf{S}^* ,$$

with modified Jacobian and source term vector

$$\mathbf{A}^* := \frac{\Delta t}{\Delta x_i} \mathbf{A}(\mathbf{Q}_h) , \quad \mathbf{S}^* := \Delta t \mathbf{S}(\mathbf{Q}_h)$$

and introduce

$$[a,b]^\tau = \int_0^1 a(\xi,\tau)\, b(\xi,\tau)\, d\xi , \quad < a,b >_{T_E} = \int_0^1 \int_0^1 a(\xi,\tau)\, b(\xi,\tau)\, d\xi d\tau .$$

Dumbser-Enaux-Toro Solver

Use a space-time basis function $\theta = \theta(\xi, \tau)$ to multiply, integrate over T_E and integrate by parts the time derivative term

$$[\theta, \mathbf{Q}_h]^1 - \langle \partial_\tau \theta, \mathbf{Q}_h \rangle_{T_E} + \langle \theta, \mathbf{A}^* \partial_\xi \mathbf{Q}_h \rangle_{T_E} = [\theta, \mathbf{w}_h]^0 + \langle \theta, \mathbf{S}^* \rangle_{T_E} .$$

Use same space-time basis functions θ for $\mathbf{Q}_h$ and $\mathbf{A}^* \partial_\xi \mathbf{Q}_h$, so that

$$\mathbf{Q}_h(\xi, \tau) = \sum_{l=1}^{(M+1)^2} \theta_l \hat{\mathbf{Q}}_l , \quad \mathbf{A}^* \partial_\xi \mathbf{Q}_h(\xi, \tau) = \sum_{l=1}^{(M+1)^2} \theta_l \widehat{\mathbf{A}^* \partial_\xi \mathbf{Q}}_l .$$

Dumbser-Enaux-Toro Solver

Solve the resulting system by a fixed point iteration procedure

$$\left([\theta_k,\theta_l]^1 - \langle \partial_\tau \theta_k, \theta_l \rangle_{T_E}\right) \hat{\mathbf{Q}}_l^{m+1} - \langle \theta_k, \theta_l \rangle_{T_E} \mathbf{S}^*(\hat{\mathbf{Q}}_l^{m+1}) = [\theta_k,\psi_l]^0 \hat{\mathbf{w}}_l - \langle \theta_k, \theta_l \rangle_{T_E} \widehat{\mathbf{A}^* \partial_\xi \mathbf{Q}}_l^m ,$$

for $k = 1, 2, \ldots, (M+1)^2$.

- Solution to GRP at time τ is found by solving a classical Riemann problem using $\mathbf{Q}_h(\xi,\tau)$ at both sides of the cell interface (Montecinos et al., 2012).
- Space-time integrals of $\mathbf{A}(\mathbf{Q})\partial_x \mathbf{Q}$ and $\mathbf{S}(\mathbf{Q})$ are computed by numerical integration using $\mathbf{Q}_h(\xi,\tau)$ and a quadrature rule of appropriate accuracy. (Hidalgo and Dumbser, 2011).

Dumbser-Enaux-Toro Solver

Solve the resulting system by a fixed point iteration procedure

$$\left([\theta_k,\theta_l]^1 - \langle \partial_\tau \theta_k, \theta_l \rangle_{T_E}\right) \hat{\mathbf{Q}}_l^{m+1} - \langle \theta_k, \theta_l \rangle_{T_E} \mathbf{S}^*(\hat{\mathbf{Q}}_l^{m+1}) = [\theta_k,\psi_l]^0 \hat{\mathbf{w}}_l - \langle \theta_k, \theta_l \rangle_{T_E} \widehat{\mathbf{A}^* \partial_\xi \mathbf{Q}}_l^m ,$$

for $k = 1, 2, \ldots, (M+1)^2$.

- Solution to GRP at time τ is found by solving a classical Riemann problem using $\mathbf{Q}_h(\xi, \tau)$ at both sides of the cell interface (Montecinos et al., 2012).
- Space-time integrals of $\mathbf{A}(\mathbf{Q})\partial_x \mathbf{Q}$ and $\mathbf{S}(\mathbf{Q})$ are computed by numerical integration using $\mathbf{Q}_h(\xi, \tau)$ and a quadrature rule of appropriate accuracy. (Hidalgo and Dumbser, 2011).

Dumbser-Enaux-Toro Solver

Solve the resulting system by a fixed point iteration procedure

$$\left([\theta_k,\theta_l]^1 - \langle \partial_\tau \theta_k, \theta_l \rangle_{T_E}\right) \hat{\mathbf{Q}}_l^{m+1} - \langle \theta_k, \theta_l \rangle_{T_E} \mathbf{S}^*(\hat{\mathbf{Q}}_l^{m+1}) = [\theta_k,\psi_l]^0 \hat{\mathbf{w}}_l - \langle \theta_k, \theta_l \rangle_{T_E} \widehat{\mathbf{A}^* \partial_\xi \mathbf{Q}}_l^m ,$$

for $k = 1, 2, \ldots, (M+1)^2$.

- Solution to GRP at time τ is found by solving a classical Riemann problem using $\mathbf{Q}_h(\xi, \tau)$ at both sides of the cell interface (Montecinos et al., 2012).
- Space-time integrals of $\mathbf{A}(\mathbf{Q})\partial_x \mathbf{Q}$ and $\mathbf{S}(\mathbf{Q})$ are computed by numerical integration using $\mathbf{Q}_h(\xi, \tau)$ and a quadrature rule of appropriate accuracy. (Hidalgo and Dumbser, 2011).

Validation: convergence tests

We prescribe a smooth function $\hat{\mathbf{Q}}(x,t)$

$$\hat{\mathbf{Q}}(x,t) = [\hat{A}(x,t), \hat{q}(x,t), \hat{\theta}(x,t), \hat{A}_0(x,t), \hat{h}_0(x,t), \hat{E}_e(x), \hat{E}_c(x), \hat{p}_e(x)]^T ,$$

to be the solution of

$$\partial_t \mathbf{Q} + \mathbf{A}(\mathbf{Q})\partial_x \mathbf{Q} = \hat{\mathbf{S}}(x,t) ,$$

where $\hat{\mathbf{S}}(x,t)$ reflects the fact that $\hat{\mathbf{Q}}(x,t)$ is not a solution of the original system.

Validation: convergence tests

ADER-O2

T [s]	N	L^1	L^2	L^∞	$\mathcal{O}(L^1)$	$\mathcal{O}(L^2)$	$\mathcal{O}(L^\infty)$	Δ
10^{-2} & $K_m \approx 0$	4	2.63e-07	2.96e-07	5.25e-07	-	-	-	
	8	5.82e-08	6.87e-08	1.80e-07	2.2	2.1	1.5	1.03e-01
	16	1.40e-08	1.72e-08	4.69e-08	2.1	2.0	1.9	4.10e-01
	32	3.20e-09	4.04e-09	1.23e-08	2.1	2.1	1.9	1.64e+00
	64	7.74e-10	9.94e-10	3.17e-09	2.0	2.0	2.0	6.56e+00
	128	1.87e-10	2.41e-10	7.47e-10	2.0	2.0	2.1	2.62e+01
	256	4.65e-11	6.00e-11	1.87e-10	2.0	2.0	2.0	1.05e+02
10^{-2}	4	2.46e-07	2.94e-07	6.57e-07	-	-	-	
	8	5.55e-08	6.91e-08	2.01e-07	2.1	2.1	1.7	1.03e-01
	16	1.29e-08	1.66e-08	5.09e-08	2.1	2.1	2.0	4.10e-01
	32	3.30e-09	4.05e-09	1.14e-08	2.0	2.0	2.2	1.64e+00
	64	1.70e-09	2.08e-09	4.36e-09	1.0	1.0	1.4	6.56e+00
	128	1.92e-09	2.13e-09	3.51e-09	-0.2	-0.0	0.3	2.62e+01
	256	1.98e-09	2.19e-09	3.36e-09	-0.0	-0.0	0.1	1.05e+02
10^{-3}	4	2.46e-07	2.98e-07	6.74e-07	-	-	-	
	8	5.29e-08	7.58e-08	2.41e-07	2.2	2.0	1.5	1.03e-02
	16	1.28e-08	1.90e-08	6.47e-08	2.0	2.0	1.9	4.10e-02
	32	3.13e-09	4.67e-09	1.62e-08	2.0	2.0	2.0	1.64e-01
	64	7.48e-10	1.08e-09	3.85e-09	2.1	2.1	2.1	6.56e-01
	128	1.97e-10	2.44e-10	7.34e-10	1.9	2.2	2.4	2.62e+00
	256	1.63e-10	1.88e-10	3.52e-10	0.3	0.4	1.1	1.05e+01

Empirical convergence rates for a second order ADER scheme with several relaxation times T. N is the number of cells. Errors are computed for variable A. The highlighted row corresponds to the largest number of cells N for which the theoretical convergence rate is achieved.

Validation: convergence tests

ADER-O3

T [s]	N	L^1	L^2	L^∞	$\mathcal{O}(L^1)$	$\mathcal{O}(L^2)$	$\mathcal{O}(L^\infty)$	Δ
10^{-2} & $K_m \approx 0$	4	1.14e-07	1.29e-07	1.94e-07	-	-	-	
	8	1.37e-08	1.66e-08	3.44e-08	3.1	3.0	2.5	3.22e-01
	16	1.84e-09	2.22e-09	4.73e-09	2.9	2.9	2.9	2.58e+00
	32	2.22e-10	2.71e-10	6.15e-10	3.1	3.0	2.9	2.06e+01
	64	2.77e-11	3.40e-11	8.21e-11	3.0	3.0	2.9	1.65e+02
	128	3.51e-12	4.35e-12	1.14e-11	3.0	3.0	2.8	1.32e+03
	256	4.84e-13	6.08e-13	1.71e-12	2.9	2.8	2.7	1.06e+04
10^{-2}	4	9.15e-08	1.06e-07	2.07e-07	-	-	-	
	8	1.35e-08	1.64e-08	3.44e-08	2.8	2.7	2.6	3.22e-01
	16	2.85e-09	3.24e-09	5.93e-09	2.2	2.3	2.5	2.58e+00
	32	2.03e-09	2.25e-09	3.45e-09	0.5	0.5	0.8	2.06e+01
	64	2.01e-09	2.22e-09	3.33e-09	0.0	0.0	0.1	1.65e+02
	128	2.01e-09	2.22e-09	3.31e-09	-0.0	0.0	0.0	1.32e+03
	256	2.01e-09	2.22e-09	3.31e-09	-0.0	0.0	0.0	1.06e+04
10^{-3}	4	1.03e-07	1.31e-07	2.32e-07	-	-	-	
	8	1.28e-08	1.58e-08	3.42e-08	3.0	3.0	2.8	3.22e-02
	16	1.67e-09	2.09e-09	4.71e-09	2.9	2.9	2.9	2.58e-01
	32	3.06e-10	3.50e-10	6.85e-10	2.5	2.6	2.8	2.06e+00
	64	2.04e-10	2.27e-10	3.56e-10	0.6	0.6	0.9	1.65e+01
	128	2.02e-10	2.24e-10	3.38e-10	0.0	0.0	0.1	1.32e+02
	256	2.02e-10	2.24e-10	3.35e-10	-0.0	0.0	0.0	1.06e+03

Empirical convergence rates for a third order ADER scheme with several relaxation times T. N is the number of cells. Errors are computed for variable A. The highlighted row corresponds to the largest number of cells N for which the theoretical convergence rate is achieved.

Validation: exact vs numerical Riemann problem solutions

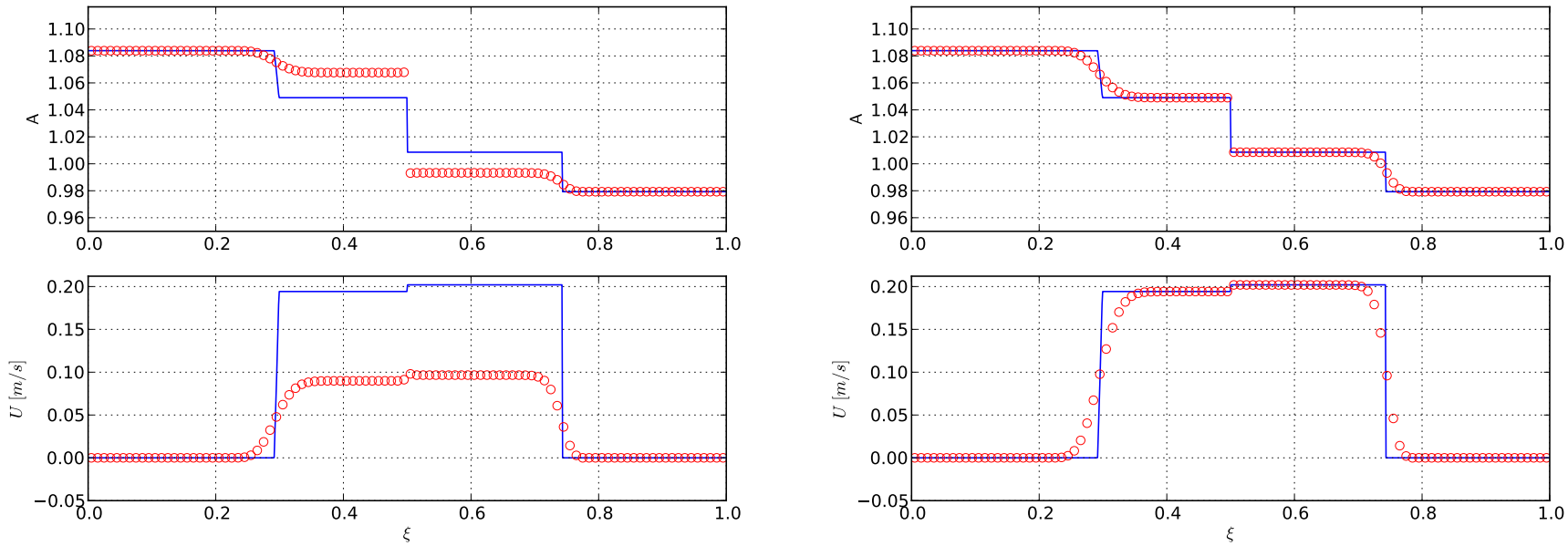

Exact and first order numerical solutions for a Riemann problem. The left and right columns show results obtained using a non well-balanced scheme and the proposed path , respectively.

Current and future work

- Further development of numerical schemes
- Implementation of the above-described numerical schemes in the General Purpose Parallel Solver (HemoLab in-house code)
- Exploring further algorithm optimization by the use of local time-stepping (Castro et al., 2009)

Final remarks

- ADAN poses numerical and data management/mining challenges
- Numerical challenges are being addressed
- Big data remains an open issue

... and last but not least ...

Above presented high-order FV methods can be applied to other problems in multiple spatial dimensions

Final remarks

- ADAN poses numerical and data management/mining challenges
- Numerical challenges are being addressed
- Big data remains an open issue

... and last but not least ...

Above presented high-order FV methods can be applied to other problems in multiple spatial dimensions

See more at

http://hemolab.lncc.br/adan-web

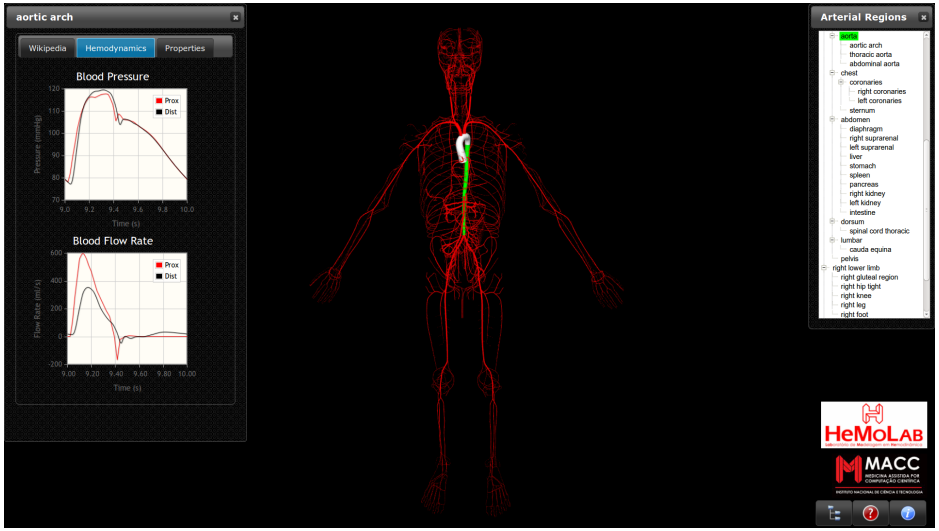

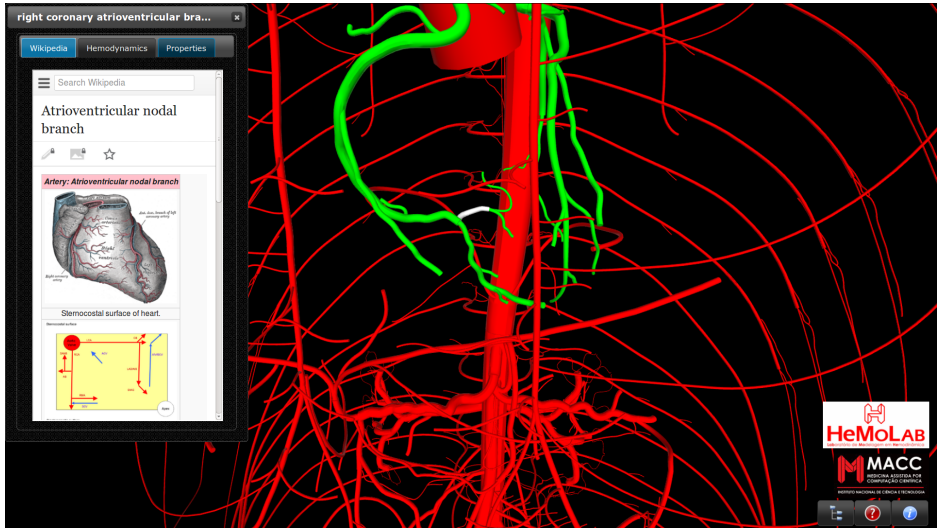

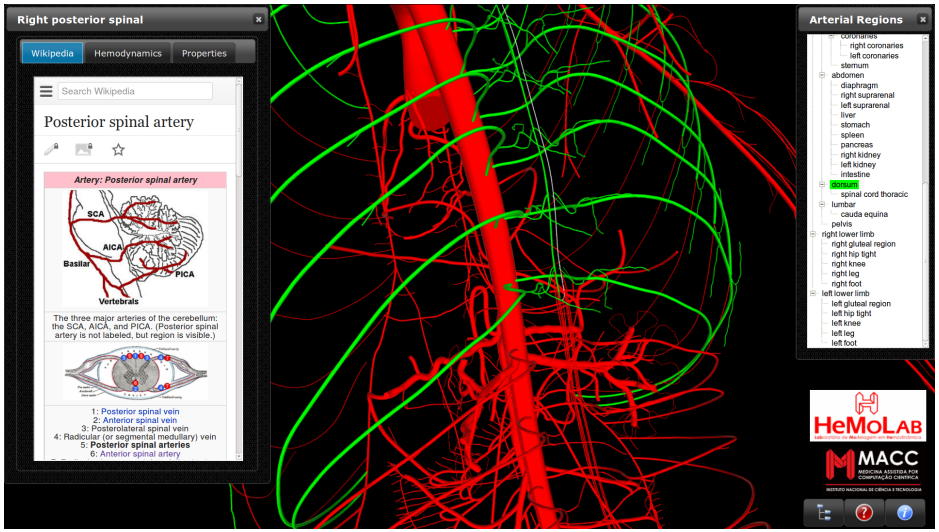

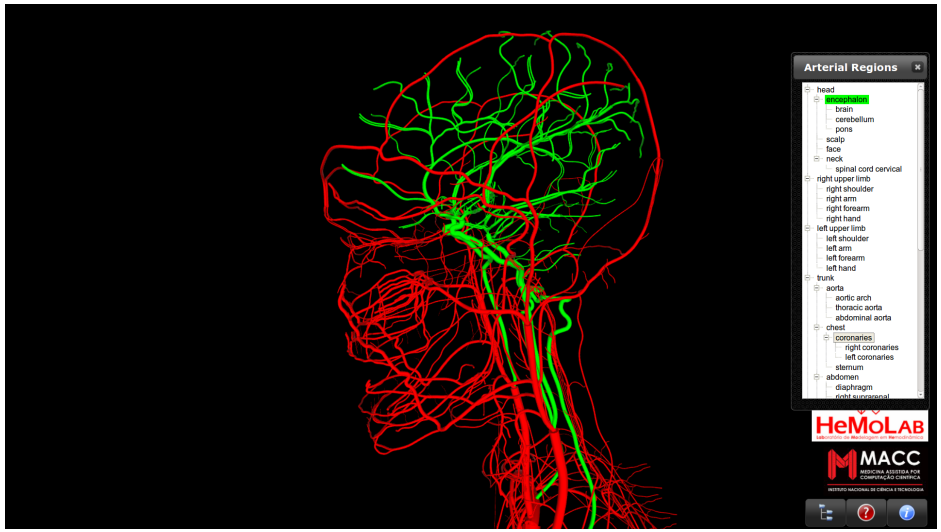

Thank you for your attention!

References I

P. J. Blanco, P. R. Trenhago, L. G. Fernandes, and R. A. Feijóo. On the integration of the baroreflex control mechanism in a heterogeneous model of the cardiovascular system. *International Journal for Numerical Methods in Biomedical Engineering*, 28(4):412–433, 2012.

C. E. Castro, M. Kser, and E. F. Toro. Spacetime adaptive numerical methods for geophysical applications. *Philosophical Transactions of the Royal Society A: Mathematical,Physical and Engineering Sciences*, 367(1907):4613–4631, 2009.

P. Chen, A. Quarteroni, and G. Rozza. Uncertainty quantification of the human arterial network. Technical Report 55, MOX.

G. Dal Maso, P. G. LeFloch, and F. Murat. Definition and weak stability of nonconservative products. *Journal de Mathématiques Pures et Appliquées*, 74:483–548, 1995.

M. Dumbser and E. F. Toro. A Simple Extension of the Osher Riemann Solver to Non-conservative Hyperbolic Systems. *Journal of Scientific Computing*, 48:70–88, 2011.

M. Dumbser, D. S. Balsara, E. F. Toro, and C. Munz. A unified framework for the construction of one-step finite volume and discontinuous Galerkin schemes on unstructured meshes. *Journal of Computational Physics*, 227:8209–8253, 2008a.

M. Dumbser, C. Enaux, and E. F. Toro. Finite volume schemes of very high order of accuracy for stiff hyperbolic balance laws. *Journal of Computational Physics*, 227:3971–4001, 2008b.

A. Hidalgo and M. Dumbser. ADER Schemes for Nonlinear Systems of Stiff Advection-Diffusion-Reaction Equations. *Journal of Scientific Computing*, 48:173–189, 2011.

G. Jiang and C. Shu. Efficient Implementation of Weighted ENO Schemes. *Journal of Computational Physics*, 126:202–228, 1996.

D. Lombardi. Inverse problems in 1d hemodynamics on systemic networks: A sequential approach. *International Journal for Numerical Methods in Biomedical Engineering*, pages n/a–n/a, 2013.

V. Martin, F. Clément, A. Decoene, and J. Gerbeau. Parameter identification for a one-dimensional blood flow model. *ESAIM: Proc.*, 14:174–200, 2005.

G. Montecinos, L. Müller, and E. F. Toro. Hyperbolic reformulation of a 1D viscoelastic blood flow model and ADER finite volume schemes. *Journal of Computational Physics*, 266:101–123, 2014.

References II

G. I. Montecinos and E. F. Toro. Reformulations for general advection-diffusion-reaction equations and locally implicit ADER schemes. *Journal of Computational Physics*, (0):–, 2014.

G. I. Montecinos, C. E. Castro, M. Dumbser, and E. F. Toro. Comparison of solvers for the generalized Riemann problem for hyperbolic systems with source terms. *Journal of Computational Physics*, 231:6472–6494, 2012.

L. O. Müller and E. F. Toro. Well-balanced high-order solver for blood flow in networks of vessels with variable properties. *International Journal for Numerical Methods in Biomedical Engineering*, 29:1388–1411, 2013.

E. F. Toro and A. Siviglia. Flow in collapsible tubes with discontinuous mechanical properties: mathematical model and exact solutions. *Communications in Computational Physics*, 13(2):361–385, 2013.

Some considerations on the efficiency of high-order schemes

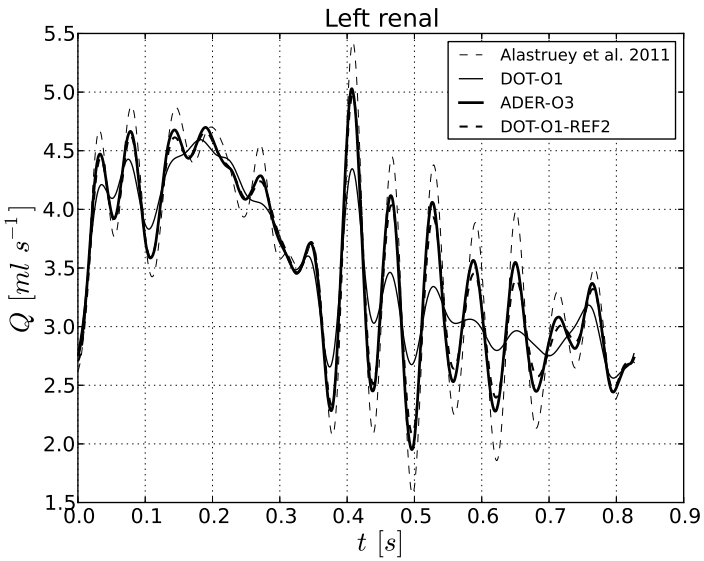

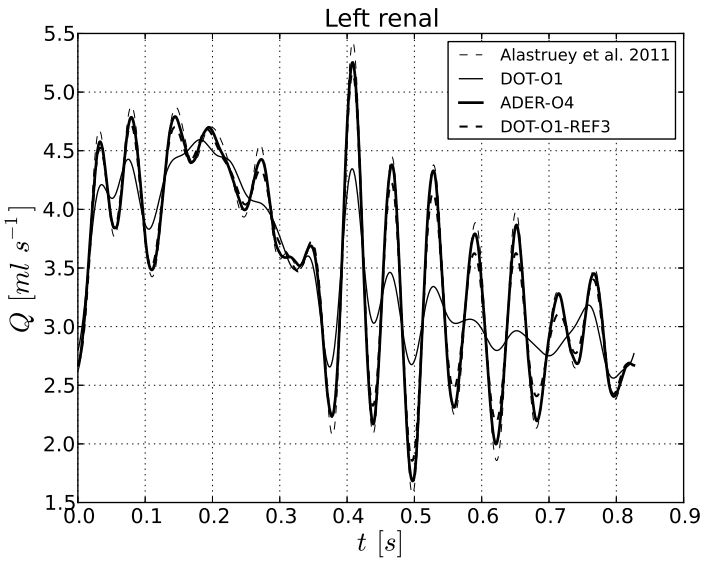

Comparison of numerical results obtained with the first-order scheme on refined grids and with the higher order implementations on the original grid. See Müller and Toro (2013) for details.

Some considerations on the efficiency of high-order schemes

Tests	nDOF	$\Delta x\,[cm]$	$t_{cpu}\,[s]$
DOT-O1	-	2	3.11
DOT-O1-REF1	-	1	17.78
DOT-O1-REF2	-	0.5	53.82
DOT-O1-REF3	-	0.25	151.31
ADER-O2	1124	2	4.60
ADER-O3	2529	2	8.99
ADER-O4	4496	2	21.37

Computational cost for different runs. See Müller and Toro (2013) for details.

One-step discontinuous Galerkin schemes

The ADER-DG scheme (Dumbser et al., 2008a) is a fully discrete DG scheme that evolves a space polynomial $\mathbf{u}_h^n = \psi_l(\xi)\hat{\mathbf{u}}_l^n$ defined in each computational cell T_i.

The solution at time t^{n+1} is obtained from

$$[\psi_k,\psi_l]^1\hat{\mathbf{u}}_l^{n+1} - [\psi_k,\psi_l]^0\hat{\mathbf{u}}_l^n + \langle\psi_k,\theta_l\rangle_{T_E}\widehat{\mathbf{A}^*\partial_\xi\mathbf{Q}}_l - \langle\psi_k,\theta_l\rangle_{T_E}\mathbf{S}^*(\hat{\mathbf{Q}}_l) + \{\psi_k,\mathcal{D}^-_{i+\frac{1}{2}}\}^1 + \{\psi_k,\mathcal{D}^+_{i-\frac{1}{2}}\}^0 = 0\,,$$

for $k = 1, 2, \ldots, M+1$, with $\hat{\mathbf{Q}}_l$ computed with the DET solver and

$$\{a,b\}^\xi = \int_0^1 a(\xi,\tau)\,b(\xi,\tau)\,d\tau\,.$$

One-step discontinuous Galerkin schemes

The ADER-DG scheme (Dumbser et al., 2008a) is a fully discrete DG scheme that evolves a space polynomial $\mathbf{u}_h^n = \psi_l(\xi)\hat{\mathbf{u}}_l^n$ defined in each computational cell T_i.

The solution at time t^{n+1} is obtained from

$$[\psi_k, \psi_l]^1 \hat{\mathbf{u}}_l^{n+1} - [\psi_k, \psi_l]^0 \hat{\mathbf{u}}_l^n + \langle \psi_k, \theta_l \rangle_{T_E} \widehat{\mathbf{A}^* \partial_\xi \mathbf{Q}}_l - \langle \psi_k, \theta_l \rangle_{T_E} \mathbf{S}^*(\hat{\mathbf{Q}}_l) + \{\psi_k, \mathcal{D}^-_{i+\frac{1}{2}}\}^1 + \{\psi_k, \mathcal{D}^+_{i-\frac{1}{2}}\}^0 = 0\,,$$

for $k = 1, 2, \ldots, M+1$, with $\hat{\mathbf{Q}}_l$ computed with the DET solver and

$$\{a, b\}^\xi = \int_0^1 a(\xi, \tau)\, b(\xi, \tau)\, d\tau\,.$$